Physica D 336 (2016) 53–61

Contents lists available at ScienceDirect

Physica D

journal homepage: www.elsevier.com/locate/physd

Modulational instability in a *PT*-symmetric vector nonlinear Schrödinger system

J.T. Cole [a,*], K.G. Makris [b], Z.H. Musslimani [a], D.N. Christodoulides [c], S. Rotter [d]

[a] Department of Mathematics, Florida State University, Tallahassee, FL 32306, USA
[b] Crete Center for Quantum Complexity and Nanotechnology, Department of Physics, University of Crete, P.O. Box 2208, 71003, Heraklion, Greece
[c] College of Optics/CREOL, University of Central Florida, Orlando, FL 32816, USA
[d] Institute for Theoretical Physics, Vienna University of Technology (TU Wien), A-1040 Vienna, Austria

HIGHLIGHTS

- Exact constant intensity solutions to a vector NLS system with *PT*-symmetric potential are constructed.
- Wave solutions propagate without scattering despite the presence of gain and loss.
- A linear stability analysis reveals the existence of an intensity threshold for instability development.
- Direct numerical simulations confirm the stability analysis and reveal the formation of coherent structures.

ARTICLE INFO

Article history:
Received 6 March 2016
Accepted 1 July 2016
Available online 16 July 2016
Communicated by V.M. Perez-Garcia

Keywords:
Vector NLS system
PT-symmetric potential
Modulational instability

ABSTRACT

A class of exact multi-component constant intensity solutions to a vector nonlinear Schrödinger (NLS) system in the presence of an external *PT*-symmetric complex potential is constructed. This type of uniform wave pattern displays a non-trivial phase whose spatial dependence is induced by the lattice structure. In this regard, light can propagate without scattering while retaining its original form despite the presence of inhomogeneous gain and loss. These constant-intensity continuous waves are then used to perform a modulational instability analysis in the presence of both non-hermitian media and cubic nonlinearity. A linear stability eigenvalue problem is formulated that governs the dynamical evolution of the periodic perturbation and its spectrum is numerically determined using Fourier–Floquet–Bloch theory. In the self-focusing case, we identify an intensity threshold above which the constant-intensity modes are modulationally unstable for any Floquet–Bloch momentum belonging to the first Brillouin zone. The picture in the self-defocusing case is different. Contrary to the bulk vector case, where instability develops only when the waves are *strongly* coupled, here an instability occurs in the strong and weak coupling regimes. The linear stability results are supplemented with direct (nonlinear) numerical simulations.

1. Introduction

Modulational instability (MI) is a special type of symmetry breaking instability [1] whereby a uniform in space intensity solution to some underlying evolution equation disintegrates due to the intricate interplay between external perturbations (e.g. random noise), dispersion/diffraction and nonlinearity. The instability manifests itself in the appearance of a nonlinear coherent structure that, in many realistic cases, takes the form of a periodic wave pattern. Historically speaking, it was first theoretically predicted and experimentally observed in the context of fluid mechanics [2,3]. Soon thereafter it was realized that modulational instability is rather a universal phenomenon that exists in many other branches of nonlinear sciences, such as biology, chemistry [4,5], plasma physics [6] and nonlinear optics [7–12] (see [13] for a more in-depth history of MI).

Another type of modulational instability that exists in higher dimensions is the so-called transverse instability. Here, the solution to a two-dimensional governing equation is uniform in one space dimension and displays some nontrivial spatial structure in the other. It was first identified by Zakharov and Rubenchik in the context of the two-dimensional nonlinear Schrödinger (NLS) equation [14] and has been predicted and observed in many

* Corresponding author.
E-mail address: jcole@math.fsu.edu (J.T. Cole).

http://dx.doi.org/10.1016/j.physd.2016.07.001
0167-2789/

research areas such as fluid mechanics [15,16], Bose–Einstein condensates [17–20] and nonlinear optics [21–23] (see [24] for a review).

Recently, there has been a resurgent mathematical and computational interest in the modulational instability problem associated with the nonlinear Schrödinger equation. In particular, special emphasis has been placed on the nonlinear evolution stage and long-time dynamics (beyond the linear stability regime). In particular, Zakharov and Gelash [25,26] as well as Biondini and Mantzavinos [27] have studied the nonlinear MI process by solving the focusing NLS equation with nonzero boundary conditions on the whole real line using the inverse scattering transform method [28].

In most theoretical studies of modulational instability the underlying evolution equations are mathematically modeled by nonlinear partial differential equations (PDEs) with constant coefficients that simplify the analysis since constant-intensity (CI) solutions are readily obtained. Physically, this corresponds to wave propagation in homogeneous media. The problem of modulational instability becomes significantly more difficult (both conceptually and mathematically) for waves propagating in inhomogeneous nonlinear media where now the underlying dynamical models are non-constant coefficient PDEs. A typical example is the Gross–Pitaevskii (or NLS) equation

$$i\varphi_z + \varphi_{xx} + V(x)\varphi + g|\varphi|^2\varphi = 0, \tag{1}$$

where φ is a complex wave function, V is a *real*-valued external potential and $g = 1$ (focusing nonlinearity) or $g = -1$ (defocusing nonlinearity). The difficulty here is that Eq. (1) does *not* admit solutions of the form $\varphi(x, z) = \varphi_0 \exp(ikx + i\kappa z)$ where φ_0 is a complex amplitude independent of x and z, k is the wavenumber, and $\kappa = \kappa(k)$ is a real propagation constant. Hence it is impossible to carry out a true MI analysis. Note that if one allows the potential in (1) to also depend on z, then one can perform a numerical study of modulational instability as was done in [29] for a parabolic potential with a z-dependent amplitude. We point out that modulational instability of periodic (in x) solutions to Eq. (1) corresponding to periodic potentials have also been studied in the literature [30,31]. In certain limiting cases one can replace the Gross–Pitaevskii or NLS equation (1) by its asymptotic reduction which significantly simplifies the MI analysis [32]. For example, the following discrete nonlinear Schrödinger equation modeling wave propagation in waveguide arrays

$$i\frac{d\zeta_n}{dz} + \zeta_{n+1} + \zeta_{n-1} + \gamma|\zeta_n|^2\zeta_n = 0, \quad n \in \mathbb{Z}, \tag{2}$$

is obtained from Eq. (1) in the tight-binding limit [33] [see Ref. [34] for detailed derivation of Eq. (2)]. The constant intensity solutions to Eq. (2) are readily found by substituting the ansatz $\zeta_n(z) = \tilde{\zeta}\exp(i\sigma z + iQn)$, where σ, Q, γ and $\tilde{\zeta}$ are real constants.

Over the last few years there has been an intense theoretical [35–39] and experimental [40–42] research interest in the general area of optical wave propagation in linear and nonlinear media with balanced gain and loss. Such wave phenomena are modeled by the nonlinear Schrödinger equation (1) where now the external potential V is assumed to be *complex* and satisfies the so-called parity-time (PT)-symmetry condition [43,44]

$$V^*(x) = V(-x), \tag{3}$$

where * denotes complex conjugation. Allowing the potential V to become complex-valued opens up many opportunities to explore intriguing wave dynamics that do not exist otherwise. The concept of an exceptional point is one such important example that exists only in non-hermitian systems and has lead to many novel physical applications such as PT-synthetic lattices [45], unidirectional invisibility [46], photonic molecule lasers [47,48], and optical isolators [49,50].

Building upon these parity-time symmetry concepts, recently modulational instability of constant-intensity solutions to the nonlinear Schödinger equation (1) in the presence of the general class of complex potentials

$$V(x) = W^2(x) - i\frac{dW}{dx}, \tag{4}$$

where W is a smooth and real-valued function, was studied for the first time in [51]. In this case, constant intensity solutions are obtained in the form

$$\varphi(x, z) = \varphi_0 e^{ig\varphi_0^2 z + i\int_0^x W(\xi)d\xi}, \tag{5}$$

with constant and real amplitude φ_0. In [51], it was shown that for the self-focusing case all large amplitude CI waves (5) are unstable to modulated perturbations. Furthermore, it was numerically observed that CI waves are weakly unstable in the self-defocusing regime. This is contrary to the bulk ($V(x) = 0$) case where no MI exists. Direct numerical simulations revealed that periodic perturbations forced the CI waves to disintegrate into a train of nonlinear coherent structures.

We would also like to point out that modulational instability in the nonlinear Schrödinger equation with only linear losses has been considered in the context of weakly nonlinear water waves [52]. There, it was found that any amount of a certain type of dissipation arrested all MI development. Thus the presence of a complex potential can lead to many unexpected and perhaps counterintuitive outcomes.

It is well known that nonlinear wave coupling can lead to many new and fascinating physical phenomena. In this regard, the dynamical evolution equations describing two interacting paraxial waves propagating in inhomogeneous nonlinear Kerr media are given by the following dimensionless vector NLS system

$$i\frac{\partial\psi}{\partial z} + \frac{\partial^2\psi}{\partial x^2} + V(x)\psi + g(|\psi|^2 + \beta|\phi|^2)\psi = 0, \tag{6}$$

$$i\frac{\partial\phi}{\partial z} + \frac{\partial^2\phi}{\partial x^2} + V(x)\phi + g(\beta|\psi|^2 + |\phi|^2)\phi = 0, \tag{7}$$

where ψ and ϕ are complex-valued envelope functions, z is the propagation direction, $g = \pm 1$, and $\beta \geq 0$ is the cross-phase modulation coefficient. For example, in the homogeneous case ($V = 0$) the cross-phase modulation term β can generate an instability (of plane waves) that otherwise would be stable [53,54] (see Appendix). Vector solitons in the form of bright–bright, bright–dark, or dark–dark have also been theoretically and experimentally observed in many settings [55,56].

In this paper we study modulational instability of vector constant-intensity solutions to system (6) and (7) in the presence of a complex PT-symmetric potential. The main results of this paper are:

- Construction of vector CI waves with nonlinear spatial phase to system (6) and (7) in the presence of a PT-symmetric complex potential.
- Formulation of a linear eigenvalue problem whose unstable spectrum is computed using a Fourier–Floquet–Bloch method.
- The existence of a threshold intensity above which vector CI waves are unstable.
- Identification of certain ring-type regions in wave amplitude space where CI solutions become modulationally unstable in the self-defocusing case.
- Direct numerical simulations of vector MI beyond the linear stability regime.

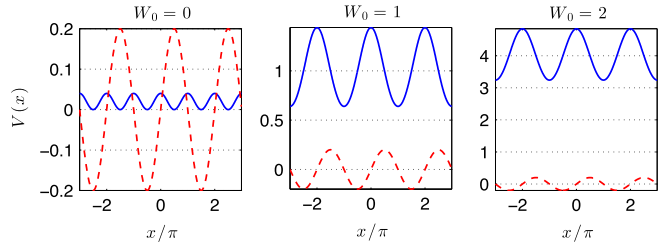

Fig. 1. The real (solid blue lines) and imaginary (red dashed lines) parts of complex potential (4) for $W_1 = 0.1$ and different integer values of W_0.

This paper is organized as follows: In the next section we give a closed form solution to system (6) and (7) whose intensity is uniform in space. In Section 3, we investigate the spectral properties of PT-symmetric potential (4) for the specific example $W(x)$ given in Eq. (13). In particular, we identify regions in potential parameter space where the spectrum is entirely real. A linear stability eigenvalue problem governing the evolution of a small perturbation is derived and numerically solved in Section 4 along with a detailed discussion of the dynamical behavior of the modulational instability. A full set of nonlinear simulations that support and supplement our stability findings are given in Section 5. We conclude with an outlook for future works in Section 6.

2. Exact vector constant-intensity waves

For the system given in Eqs. (6) and (7), exact constant intensity solutions are given by

$$\psi(x,z) = Ae^{i\mu z}e^{i\theta(x)}, \tag{8}$$

$$\phi(x,z) = Be^{i\nu z}e^{i\theta(x)}, \tag{9}$$

$$\theta(x) = \int_0^x W(\xi)d\xi, \tag{10}$$

$$\mu = g(A^2 + \beta B^2), \tag{11}$$

$$\nu = g(\beta A^2 + B^2), \tag{12}$$

where A and B are constant amplitudes taken, for simplicity, to be real. We may think of this solution set as a PT-symmetric extension of the corresponding bulk plane wave modes (W = constant) with chirped spatial phase. While the solutions given in (8) and (9) are valid for any real-valued and differentiable function W, based on physical arguments (such as the requirement that the spectrum of the linear problem associated with Eq. (6) be entirely real) it is reasonable to choose V to satisfy the PT-symmetry condition (3). This in turn restricts the choice of W to be even. Throughout the rest of the paper, we shall consider the representative periodic potential [51]

$$W(x) = W_0 + 2W_1\cos x, \tag{13}$$

with non-negative coefficients W_0 and W_1. In this case, the spatial phase (10) is given by

$$\theta(x) = W_0 x + 2W_1\sin x. \tag{14}$$

The periodicity requirement $\psi(x+2\pi,z) = \psi(x,z)$ (similarly for ϕ) implies W_0 is an integer. Typical potential profiles are shown in Fig. 1.

3. Linear spectral bands

We start the analysis by first examining the spectral properties of low-intensity solutions to Eq. (6) in the form $\psi(x,z) = \varepsilon\Psi(x)e^{iEz}$ (a similar ansatz holds for ϕ), where $|\varepsilon| \ll 1$ and E is the propagation constant. To leading order in ε, the wavefunction Ψ satisfies the eigenvalue problem

$$\mathcal{L}\Psi = E\Psi, \qquad \mathcal{L} \equiv \frac{\partial^2}{\partial x^2} + V(x). \tag{15}$$

Since the operator $\mathcal{L}$ is not self-adjoint with respect to the $L^2([0,2\pi])$ inner product, the eigenvalues are, in general, complex. However, as it was shown in [43,44] if the potential V is PT-symmetric, i.e., satisfies condition (3), then in certain parameter regime, the spectrum of $\mathcal{L}$ can be entirely real. Under such circumstances the question of modulational instability is physically relevant and interesting.

To compute the spectrum of $\mathcal{L}$ we numerically solve eigenvalue problem (15) using the partial wave expansion (also known as Hill's method [57,58]). The results have also been tested using spectral Fourier differentiation matrices [59]. By Floquet–Bloch theory [60], the eigenfunctions of Eq. (15) are expressed as $\Psi(q;x) = \eta(q;x)e^{iqx}$ such that $\eta(q;x+2\pi) = \eta(q;x)$, with q being the real Bloch (quasi) momentum. Substituting this ansatz into Eq. (15) yields

$$(\partial_x + iq)^2\eta + \left(W^2 - iW_x\right)\eta = E\eta. \tag{16}$$

Given that the functions $W(x)$, $V(x)$ and $\eta(x)$ are 2π-periodic, their respective Fourier series representations are given by

$$W(x) = \sum_{n=-\infty}^{\infty} W_n e^{inx}, \tag{17}$$

$$V(x) = \sum_{n=-\infty}^{\infty} V_n e^{inx}, \tag{18}$$

$$\eta(x) = \sum_{n=-\infty}^{\infty} \eta_n e^{inx}. \tag{19}$$

Since $W(x)$ is real and even, it follows from Eq. (17) that the coefficients are real and satisfy $W_n = W_{-n}$. From Eqs. (4), (17) and (18) it follows that the Fourier expansion coefficients for V satisfy

$$V_n = nW_n + \sum_m W_m W_{n-m}, \quad n \in \mathbb{Z}, \tag{20}$$

which for the W given in (13) read

$$V_0 = W_0^2 + 2W_1^2, \qquad V_{\pm1} = W_1(2W_0 \pm 1), \qquad V_{\pm2} = W_1^2, \tag{21}$$

and $V_j \equiv 0$ for $|j| \geq 3$. Thus, Eq. (16) can be rewritten in terms of an infinite set of coupled algebraic equations. Restricting the Fourier modes to the interval $|n| \leq N/2$ for some fixed large even integer N, we obtain the system

$$\mathbb{L}\vec{\eta} = E\vec{\eta}, \tag{22}$$

$$\mathbb{L}(q) = \begin{pmatrix} \mathcal{V}_{-\frac{N}{2}} & V_{-1} & V_{-2} & & & & \\ V_1 & \mathcal{V}_{-\frac{N}{2}+1} & \ddots & \ddots & & & \\ V_2 & \ddots & \ddots & & & & \\ & \ddots & & & & & \\ & & & & & V_{-2} & \\ & & & & \mathcal{V}_{\frac{N}{2}-1} & V_{-1} & \\ & & & V_2 & V_1 & \mathcal{V}_{\frac{N}{2}} & \end{pmatrix}, \tag{23}$$

for the eigenvector $\vec{\eta} = \left(\eta_{-N/2}, \ldots, \eta_{N/2}\right)^T$ and the eigenvalue E. Here, $\mathbb{L}(q)$ is an $(N+1)\times(N+1)$ matrix whose nonzero elements are shown (23) with $\mathcal{V}_n(q) \equiv V_0 - (n+q)^2$.

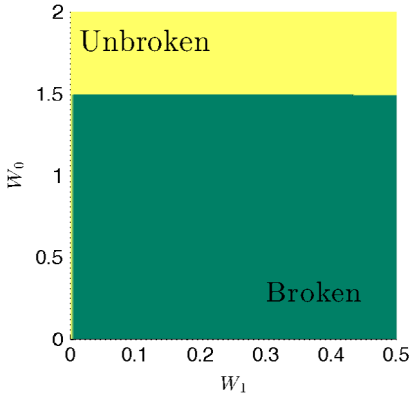

Fig. 2. Regions of broken (Im $E \neq 0$, green) and unbroken (Im $E \approx 0$, yellow) PT-symmetry computed from linear eigenvalue problem (22) with different potential parameters W_0 and W_1. (For interpretation of the references to color in this figure legend, the reader is referred to the web version of this article.)

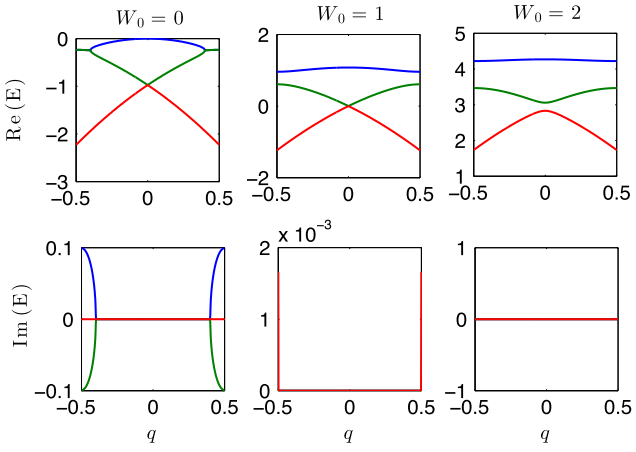

Fig. 3. Real (top) and imaginary (bottom) parts of the first three linear bands obtained from system (22) with $W_1 = 0.1$. Different colors indicate different bands ordered from top to bottom. (For interpretation of the references to color in this figure legend, the reader is referred to the web version of this article.)

Eigenvalue problem (22) is numerically diagonalized for Bloch momentum q restricted to the first Brillouin zone $[-1/2, 1/2]$. We compute the spectrum $E(q)$ corresponding to potential (13) for a wide range of potential parameters, a summary of which is shown in Fig. 2. Each point in the (W_1, W_0) plane represents an eigenvalue of the matrix $\mathbb{L}(q)$ with the largest imaginary part among all possible Bloch momenta q residing in the first Brillouin zone. We observe regions of broken (complex pairs of eigenvalues) and unbroken (real spectra) PT-symmetry. The transition boundary divides eigenvalues whose imaginary parts have magnitude less than 10^{-10} with those above this tolerance. The first three bands $E_j(q)$, $j = 1, 2, 3$ (sorted according to their real parts) are displayed in Fig. 3 for various values of W_0. As one can see, increasing the magnitude of W_0 relative to W_1 forces the spectrum to transition from being complex at the edges of the Brillouin zone, which occurs at $W_0 = 0$ and $W_0 = 1$, to pure reality at $W_0 = 2$.

4. Modulational instability

Having identified parameter regimes where the spectrum of $\mathcal{L}$ is purely real, we next focus our study on the issue of stability/instability of the CI wave solutions presented in Section 2. To that purpose, we write solutions of system (6) and (7) in the form

$$\psi(x,z) = [A + \varepsilon u(x,z)]\, e^{i\mu z + i\theta(x)}, \tag{24}$$

$$\phi(x,z) = [B + \varepsilon y(x,z)]\, e^{i\nu z + i\theta(x)}, \tag{25}$$

where $|\varepsilon| \ll 1$ measures the strength of the perturbation eigenfunction $\vec{\mathcal{U}} \equiv (u, U, y, Y)^T$ where, by definition, $U = u^*$ and $Y = y^*$. To first order in ε, one obtains the dynamical system

$$i\frac{\partial \vec{\mathcal{U}}}{\partial z} = \mathcal{M}\vec{\mathcal{U}}, \tag{26}$$

where $\mathcal{M}$ is the 4×4 matrix

$$\mathcal{M} = \begin{pmatrix} -L_A^+ & -gA^2 & -g\beta AB & -g\beta AB \\ gA^2 & L_A^- & g\beta AB & g\beta AB \\ -g\beta AB & -g\beta AB & -L_B^+ & -gB^2 \\ g\beta AB & g\beta AB & gB^2 & L_B^- \end{pmatrix}, \tag{27}$$

and

$$L_A^\pm = \partial_x^2 + gA^2 \pm 2iW\partial_x, \tag{28}$$

$$L_B^\pm = \partial_x^2 + gB^2 \pm 2iW\partial_x. \tag{29}$$

The linear stability system (26) governs the evolution (in z) of the perturbation field $\vec{\mathcal{U}}(x,z)$. Throughout the rest of the paper, the eigenvalue problem (26) is solved on the spatial domain $[-\pi, \pi]$ only and the z dependence of the perturbation is assumed to be exponential. With this in mind, we proceed by expressing the vector $\vec{\mathcal{U}}$ in terms of the Fourier–Floquet–Bloch expansion

$$\vec{\mathcal{U}}(x,z) = \sum_{n=-\infty}^{\infty} \begin{pmatrix} u_n \\ U_n \\ y_n \\ Y_n \end{pmatrix} e^{i(n+p)x + i\lambda z}, \tag{30}$$

where $\lambda = \lambda(p)$ is the stability eigenvalue dependent on the real "perturbation momentum" p. Substituting expansion (30) into system (26) yields the following infinite-dimensional set of algebraic equations

$$-(n+p)^2 u_n - 2\sum_{m=-\infty}^{\infty} W_m\,[(n-m)+p]\,u_{n-m} + g\left[A^2(u_n + U_n) + \beta AB(y_n + Y_n)\right] = \lambda u_n, \tag{31}$$

$$(n+p)^2 U_n - 2\sum_{m=-\infty}^{\infty} W_m\,[(n-m)+p]\,U_{n-m} - g\left[A^2(U_n + u_n) + \beta AB(Y_n + y_n)\right] = \lambda U_n, \tag{32}$$

$$-(n+p)^2 y_n - 2\sum_{m=-\infty}^{\infty} W_m\,[(n-m)+p]\,y_{n-m} + g\left[\beta AB(u_n + U_n) + B^2(y_n + Y_n)\right] = \lambda y_n, \tag{33}$$

$$(n+p)^2 Y_n - 2\sum_{m=-\infty}^{\infty} W_m\,[(n-m)+p]\,Y_{n-m} - g\left[\beta AB(U_n + u_n) + B^2(Y_n + y_n)\right] = \lambda Y_n, \tag{34}$$

for the Fourier coefficients u_n, U_n, y_n and Y_n where $n \in \mathbb{Z}$. The linear stability approach presented here is valid for propagation distances z much less than the typical distance Z_{lin} given by

$$Z_{\text{lin}} \equiv -\frac{\ln(\varepsilon|w|)}{|\text{Im}\,\lambda|}, \tag{35}$$

where $|w|$ measures the largest peak amplitude among the two modes u and y. The system (31)–(34) is generic in the sense that

it is valid for any periodic W. For the potential considered in Eq. (13), system (31)–(34) reduces to

$$-2W_{-1}\omega_{n+1}u_{n+1} + \left[(gA^2 - \omega_n^2) - 2W_0\omega_n\right]u_n - 2W_1\omega_{n-1}u_{n-1} + gA^2U_n + g\beta ABy_n + g\beta ABY_n = \lambda u_n, \quad (36)$$

$$-gA^2u_n - 2W_{-1}\omega_{n+1}U_{n+1} + \left[-(gA^2 - \omega_n^2) - 2W_0\omega_n\right]U_n - 2W_1\omega_{n-1}U_{n-1} - g\beta ABy_n - g\beta ABY_n = \lambda U_n, \quad (37)$$

$$g\beta ABu_n + g\beta ABU_n - 2W_{-1}\omega_{n+1}y_{n+1} + \left[(gB^2 + \omega_n^2) - 2W_0\omega_n\right]y_n - 2W_1\omega_{n-1}y_{n-1} + gB^2Y_n = \lambda y_n, \quad (38)$$

$$-g\beta ABu_n - g\beta ABU_n - gB^2y_n - 2W_{-1}\omega_{n+1}Y_{n+1} + \left[-(gB^2 - \omega_n^2) - 2W_0\omega_n\right]Y_n - 2W_1\omega_{n-1}Y_{n-1} = \lambda Y_n, \quad (39)$$

where by definition $\omega_n(p) = n + p$. Recall that for the potential $W(x)$ in Eq. (13) it follows that $W_{-1} = W_1$. Exploiting the fast decay properties of the Fourier coefficients, we find, after restricting the Fourier sum to the band-limited modes $-N/2 \le n \le N/2$, the $4(N+1) \times 4(N+1)$ eigenvalue problem

$$\lambda(p)\vec{\mathbb{U}} = \mathbb{M}(p)\vec{\mathbb{U}}, \quad (40)$$

where the eigenvector $\vec{\mathbb{U}} = \left(\vec{u}, \vec{U}, \vec{y}, \vec{Y}\right)^T$ is composed of the following vectors

$$\vec{u} = \left(u_{-N/2}, \ldots, u_{N/2}\right)^T, \quad (41)$$

$$\vec{U} = \left(U_{-N/2}, \ldots, U_{N/2}\right)^T, \quad (42)$$

$$\vec{y} = \left(y_{-N/2}, \ldots, y_{N/2}\right)^T, \quad (43)$$

$$\vec{Y} = \left(Y_{-N/2}, \ldots, Y_{N/2}\right)^T. \quad (44)$$

Furthermore, the matrix $\mathbb{M}$ is given by

$$\mathbb{M} = \begin{pmatrix} \Omega - 2\mathbb{W} & gA^2\mathbb{I} & g\beta AB\mathbb{I} & g\beta AB\mathbb{I} \\ -gA^2\mathbb{I} & -\Omega - 2\mathbb{W} & -g\beta AB\mathbb{I} & -g\beta AB\mathbb{I} \\ g\beta AB\mathbb{I} & g\beta AB\mathbb{I} & \chi - 2\mathbb{W} & gB^2\mathbb{I} \\ -g\beta AB\mathbb{I} & -g\beta AB\mathbb{I} & -gB^2\mathbb{I} & -\chi - 2\mathbb{W} \end{pmatrix}, \quad (45)$$

with $\mathbb{I}$ denoting the $(N+1) \times (N+1)$ identity matrix. Here, $\mathbb{W}$ is the $(N+1) \times (N+1)$ matrix

$$\mathbb{W} = \begin{pmatrix} W_0\omega_{-\frac{N}{2}} & W_1\omega_{-\frac{N}{2}+1} & & & \\ W_1\omega_{-\frac{N}{2}} & W_0\omega_{-\frac{N}{2}+1} & W_1\omega_{-\frac{N}{2}+2} & & \\ & W_1\omega_{-\frac{N}{2}+1} & W_0\omega_{-\frac{N}{2}+2} & \ddots & \\ & & \ddots & \ddots & W_1\omega_{\frac{N}{2}} \\ & & & W_1\omega_{\frac{N}{2}-1} & W_0\omega_{\frac{N}{2}} \end{pmatrix}, \quad (46)$$

and Ω, χ are the diagonal matrices

$$\Omega = \begin{pmatrix} gA^2 - \omega_{-\frac{N}{2}}^2 & & & \\ & gA^2 - \omega_{-\frac{N}{2}+1}^2 & & \\ & & \ddots & \\ & & & gA^2 - \omega_{\frac{N}{2}}^2 \end{pmatrix}, \quad (47)$$

$$\chi = \begin{pmatrix} gB^2 - \omega_{-\frac{N}{2}}^2 & & & \\ & gB^2 - \omega_{-\frac{N}{2}+1}^2 & & \\ & & \ddots & \\ & & & gB^2 - \omega_{\frac{N}{2}}^2 \end{pmatrix}, \quad (48)$$

where only the nonzero elements are shown. It is evident from ansatz (30) that when λ is complex the CI waves (8) and (9) are

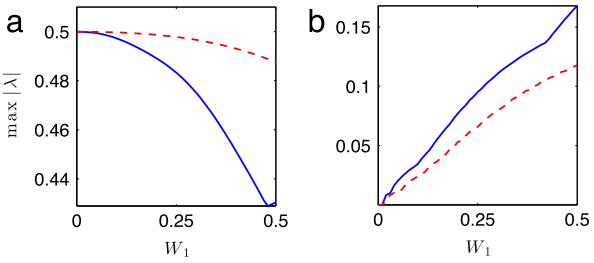

Fig. 4. The largest magnitude of the unstable eigenvalues $\lambda(p)$ scanned over all possible perturbation momenta p residing the in first Brillouin zone. Parameters are $\beta = 1, A = B = 1/2$ for (a) $g = 1$ and (b) $g = -1$. The different curves correspond to (solid blue) $W_0 = 2$ and (dashed red) $W_0 = 3$.

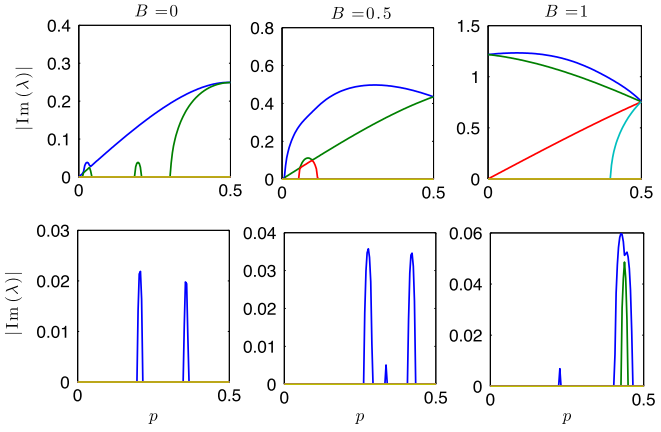

Fig. 5. The unstable eigenvalues obtained from system (40) for focusing (top) and defocusing (bottom) nonlinearities with parameters: $A = 1/2$, $W_0 = 2$, $W_1 = 0.1$ and $\beta = 1$. Different columns correspond to different values of B with each curve denoting a different band.

modulationally unstable. The unstable spectrum obtained from system (40) is computed for a wide range of potential parameters (W_1, W_0) residing in a subset of the unbroken PT-phase shown in Fig. 2 (yellow region). The largest unstable eigenvalue (representing the worst case scenario) scanned over all possible perturbation momenta p is shown in Fig. 4 for fixed values of W_0 and wave amplitude. The bulk MI results (see Appendix) are recovered when $W_1 = 0$ [54]. In the self-focusing case [see Fig. 4(a)], we identify (in general) the most unstable modes to occur in the shallow (small W_1) lattice limit. Increasing the ratio W_0/W_1, the maximum unstable eigenvalue begins to approach its bulk limit. For defocusing nonlinearity [see Fig. 4(b)] we observe regions of modulationally stable low-intensity modes existing around $W_1 = 0$. Typical examples of the unstable band modes Im (λ) as a function of the Bloch momentum p are shown in Fig. 5. Note that only the right-half of the first Brillouin zone is displayed due to reflection symmetry around $p = 0$. For focusing nonlinearities, the overall picture is that coupling leads to a stronger instability than what is observed in the scalar case. This scenario persists across the Brillouin zone. Recall that in the bulk case similar effects occur i.e. wave coupling typically leads to a more profound instability. On the other hand, for defocusing nonlinearity and in the presence of a complex potential the CI modes are also modulationally unstable though the coupling seems to have less impact than the one observed in the previous case. At larger intensities these unstable eigenvalue bands continue to resemble the isolated "humps" pattern observed in the bottom row of Fig. 5.

An interesting observation that is seen from Fig. 5 among the self-focusing bands is the absence of instability at $p = 0$ for low amplitude modes, whereas when B increases an instability

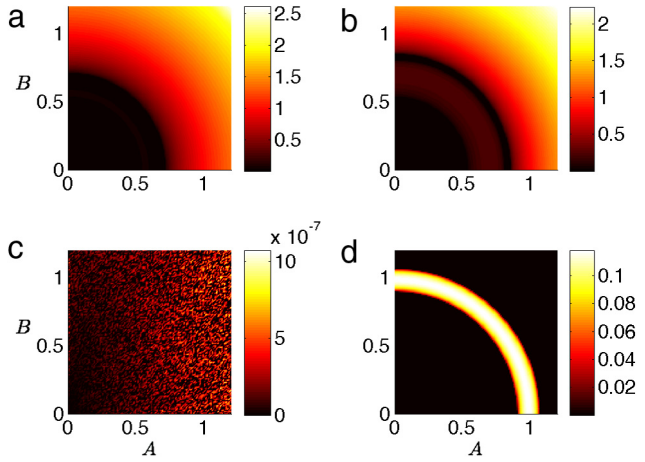

Fig. 6. The maximum magnitude of Im $\lambda(p = 0)$ obtained from Eq. (40) with (top row) focusing and (bottom row) defocusing nonlinearity. Brighter regions denote nonzero (unstable) values and black areas indicate purely real (stable) amplitudes. The other parameters are: $W_0 = 2$, $\beta = 1$ and (left column) $W_1 = 0.1$ and (right column) $W_1 = 0.4$.

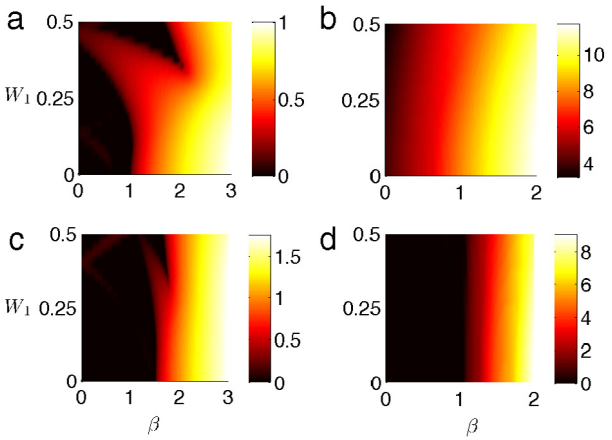

Fig. 7. The maximum magnitude of Im $\lambda(p = 0)$ obtained from Eq. (40) with (top row) focusing and (bottom row) defocusing nonlinearity for $W_0 = 2$. Brighter regions denote nonzero (unstable) values and black areas indicate purely real (stable) regions. The amplitudes are fixed at $(a)A = 1/2$, $(b)A = 2$, $(c)A = 1$, and $(d)A = 3$ (note $B = A$).

develops. To further characterize this instability and understand the role the amplitudes of the CI waves play in MI development, we compute the unstable eigenvalues Im $\lambda(p)$ at the center of the Brillouin zone ($p = 0$) for various values of A and B. A top view of the maximum unstable eigenvalue as a function of A and B is shown in Fig. 6. In the self-focusing case, near radially-symmetric contours of constant maximum unstable spectrum are observed. The black regions in Fig. 6(a) and (b) correspond to low-intensity eigenmodes with purely real (neutrally stable) eigenvalues. The dark areas indicate the existence of a threshold above which the formation of modulationally unstable modes occur. This intensity threshold for the appearance of instability also occurs in the bulk MI case (see Appendix). The instability properties for the self-defocusing case appear to be markedly different than their self-focusing counterparts. For example, in the potential parameters considered in Fig. 6(c) low-amplitude waves are found to be stable. On the other hand, increasing W_1 (i.e. more gain and loss) results in a stability threshold shown in Fig. 6(d). A bright barrier of instability, located at a (nearly) constant radial distance from the origin, separates two stable (black) regions.

Next we examine the role of the cross-phase modulation coupling β in the development of MI. For that purpose, eigenvalue system (40) is solved on a 2π-periodic domain ($p = 0$) and the largest unstable eigenvalue is displayed in Fig. 7. The striking feature in both nonlinearity types is the presence of a coupling threshold that separates stable/weakly-coupled regions (black areas) and unstable/strongly-coupled waves (bright areas). We point out that the bulk results are recovered when $W_1 = 0$. Here, there is no MI for the defocusing nonlinearity when β is less than one (see Appendix). For each of the cases considered in Fig. 7 the largest values of $|\mathrm{Im}(\lambda)|$ occur in the regions of strongest coupling. Furthermore, as the wave amplitudes increase (see right column in Fig. 7) the amount of coupling needed to excite an unstable mode decreases. Indeed, in Fig. 7(b) no coupling threshold is present.

5. Direct numerical simulations

In this section we supplement the above findings by performing several direct (nonlinear) numerical simulations. In particular, we numerically integrate Eqs. (6) and (7) with initial conditions corresponding to perturbed CI waves with 2π-periodic boundary conditions, i.e.

$$\psi(x + 2\pi, 0) = \psi(x, 0), \qquad \phi(x + 2\pi, 0) = \phi(x, 0). \tag{49}$$

This in turn implies that $p = 0$. Specifically, the initial conditions considered are of the form

$$\begin{pmatrix} \psi(x,0) \\ \phi(x,0) \end{pmatrix} = \begin{pmatrix} A \\ B \end{pmatrix} e^{i\theta(x)} + \varepsilon \begin{pmatrix} \rho(x) \\ \delta(x) \end{pmatrix}, \quad |\varepsilon| \ll 1, \tag{50}$$

where ρ and δ represent one of the following perturbation types:

- The numerically exact linear eigenmode given in Eq. (30) i.e.

$$\begin{pmatrix} \rho \\ \delta \end{pmatrix} = \begin{pmatrix} u(x,0) \\ y(x,0) \end{pmatrix} e^{i\theta(x)}, \tag{51}$$

- The tent function

$$\begin{pmatrix} \rho \\ \delta \end{pmatrix} = \begin{pmatrix} 1 - |x|/\pi \\ 1 - |x|/\pi \end{pmatrix}. \tag{52}$$

The first choice allows us to connect and test the validity of the linear stability regime, while the second one, whose Fourier modes decay slowly, should excite any unstable Fourier–Floquet modes (cf. [61]). The initial value problems (6) and (7) are numerically integrated in z using a Fourier spectral fourth-order Runge–Kutta method.

First, let us present the results pertaining to the self-focusing ($g = 1$) nonlinearity. Using the first choice of perturbation given in Eq. (51), we monitor the evolution of each individual wave as a function of the propagation distance z. The results are shown in Fig. 8. As expected, for short distances $z \ll Z_{\mathrm{lin}} \approx 2.77$, the intensities (particularly the one for ϕ) grow exponentially fast in z, after which they saturate and both waves propagate in a bounded and recurrent manner. Recall that certain low amplitude perturbation eigenvectors were predicted to be linearly stable in Fig. 6. To confirm that these modes are indeed stable and explore any nonlinear instability effects not covered in the above linear stability analysis, we perform numerical experiments using the full nonlinear system and the perturbed initial state in Eq. (50) with the tent function in (52). The findings of such a simulation for equal amplitudes are shown in Fig. 9. The dynamical wave pattern shows a bounded evolution over long distances in z. This is in contrast to the exponentially growing pulses seen in Fig. 8.

Finally, we simulate the full nonlinear system for the defocusing ($g = -1$) nonlinearity with initial disturbance given in Eqs. (50) and (51) valid when $z \ll Z_{\mathrm{lin}}$ where $Z_{\mathrm{lin}} \approx 19.49$. At these values, a weak instability is found to take place over long distances in z (see Fig. 10). Periodic intensity bursts are observed to occur in a breather-like fashion in z and this intensity pattern is observed to hold its overall form in space over the course of its evolution.

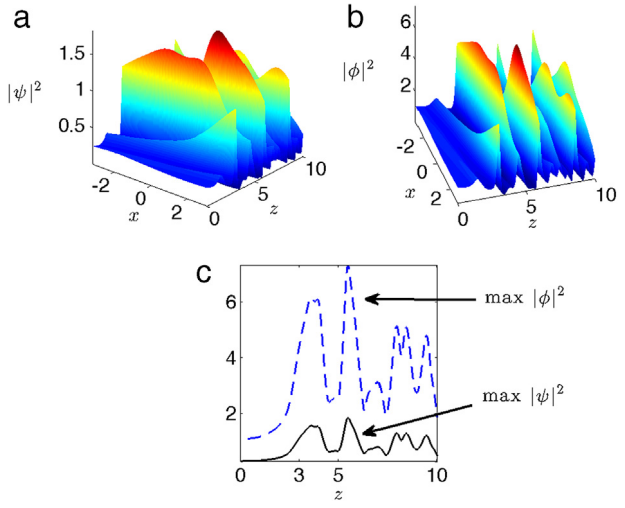

Fig. 8. Dynamic evolution of intensities (a) $|\psi|^2$ and (b) $|\phi|^2$ for the focusing nonlinear system (6)–(7) with initial perturbation given in Eqs. (50) and (51). The parameters are: $A = 1/2$, $B = 1$, $W_0 = 2$, $W_1 = 0.1$ and $\beta = 1$. The perturbation parameters are: $\varepsilon = 0.05$ and $\max_x |u(x,0)| \approx 0.343$, $\max_x |y(x,0)| \approx 0.686$ with $\lambda \approx 3.971 + 1.217i$. (c) The maximum intensity of $\psi(x,z)$ (solid black curve) and $\phi(x,z)$ (dashed blue curve) as a function of z.

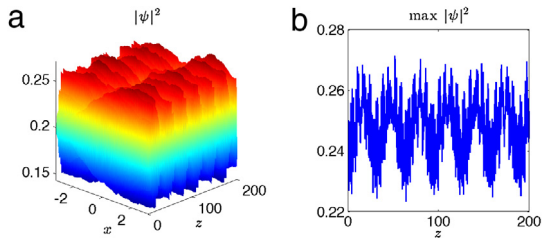

Fig. 9. (a) Dynamic evolution of focusing nonlinear system (6)–(7) with initial perturbation given in Eqs. (50) and (52). The simulation parameters are: $A = 0.45 = B$, $W_0 = 2$, $W_1 = 0.1$, $\beta = 1$, $\varepsilon = 0.05$. (b) The maximum intensity of $\psi(x,z)$ [same as $\phi(x,z)$] as a function of z.

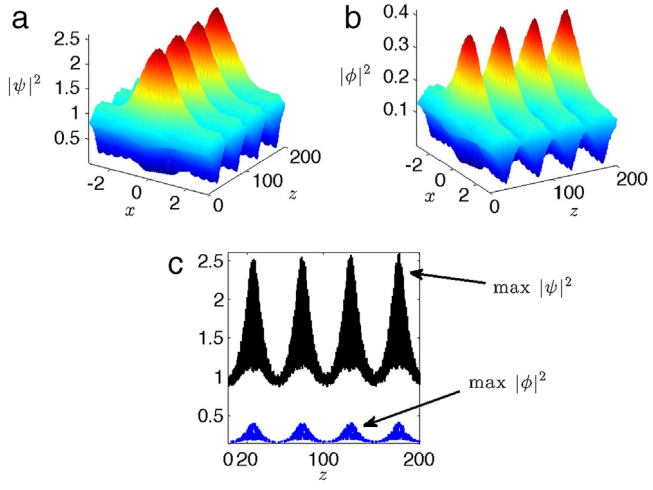

Fig. 10. Dynamic evolution of intensities (a) $|\psi|^2$ and (b) $|\phi|^2$ for the defocusing nonlinear system (6)–(7) with initial perturbation given in Eqs. (50) and (51). The problem parameters are: $A = 0.9$, $B = 0.36$, $W_0 = 2$, $W_1 = 0.4$, $\beta = 1$. The perturbation parameters are: $\varepsilon = 0.1$ and $\max_x |u(x,0)| \approx 1.045$, $\max_x |y(x,0)| \approx 0.418$ and $\lambda = 5.518 + 0.116i$. (c) The maximum intensity of $\psi(x,z)$ (solid black curve) and $\phi(x,z)$ (dashed blue curve) as a function of z. (For interpretation of the references to color in this figure legend, the reader is referred to the web version of this article.)

6. Conclusions and outlook

In this paper we presented a class of exact vector constant-intensity solutions of a two-component nonlinear Schrödinger system in the presence of a *PT*-symmetric potential. A unique feature of these solutions is their highly nonlinear phases which are directly tied to the spatial structure of the external lattice. Remarkably, such waves can propagate without distortion or reflection despite the fact that the medium, represented by the potential, is highly active, namely it has local gain and loss. This attribute is in some sense counterintuitive given the fact that the presence of obstacles should in fact lead to wave scattering and amplitude modulation.

The construction of such spatially homogeneous coupled waves allowed us to study vector modulational instability for both self-focusing and defocusing nonlinearities. Indeed, a linear stability eigenvalue problem was derived and its unstable spectrum was numerically determined using Fourier–Floquet–Bloch theory. For both types of nonlinearity we numerically observed the existence of an intensity threshold above which uniform-intensity waves are modulationally unstable. The linear stability results were supplemented with direct numerical simulations.

We note at this point, that the coupled nonlinear Schrödinger equations considered in this work, may be physically related to coupled nonlinear waveguide arrays [62] as well as two-species Bose–Einstein condensates [63–65]. These MI results, together with those obtained in [51], open many opportunities for future research directions. For example, the

- formation of *PT*-symmetric rogue waves in inhomogeneous and non-hermitian optical systems,
- extension of the present analysis to multi-dimensional scalar and vector modulational instability,
- connection between modulational instability and formation of *PT*-symmetric lattice solitons. In this regard, we note the work of [66] where solitons in *PT* symmetric potentials (4) have been constructed for *localized W*.
- study of scalar and vector modulational instability in complex potentials in the presence of four-wave mixing. In this case, Eqs. (6) and (7) become

$$i\frac{\partial\psi}{\partial z} + \frac{\partial^2\psi}{\partial x^2} + V(x)\psi + g(|\psi|^2 + \beta|\phi|^2)\psi + g_2\psi^2\phi^* = 0, \tag{53}$$

$$i\frac{\partial\phi}{\partial z} + \frac{\partial^2\phi}{\partial x^2} + V(x)\phi + g(\beta|\psi|^2 + |\phi|^2)\phi + g_2\phi^2\psi^* = 0, \tag{54}$$

where $g_2 \in \mathbb{R}$. In fact, the CI waves (8)–(12) still solve this new system with the restriction that the propagation constants μ and ν are equal, which implies that $\beta = 1$.

Acknowledgments

The work of J.T.C. and Z.H.M was supported in part by NSF Grant Number DMS-0908599. K.G.M. is supported by the People Programme (Marie Curie Actions) of the European Union's Seventh Framework Programme (FP7/2007–2013) under REA grant agreement number PIOF-GA-2011-303228 (project NOLACOME), and by the European Union Seventh Framework Programme (FP7-REGPOT-2012-2013-1) under grant agreement 316165. The work of D.N.C. was partially supported by AFSOR (FA9550-14-1-0037). S.R. acknowledges financial support by the Austrian Science Fund (FWF) through Project SFB NextLite (F49-P10) and Project GePartWave No. I 1142-N27.

Table A.1
Parameters for which it is possible for instability criteria (A.4) to be satisfied. The plus/minus signs correspond to the two signs in Eq. (A.4) where MI is possible and the null symbol indicates that no MI is possible.

	$0 < \|\beta\| < 1$	$\|\beta\| = 1$	$\|\beta\| > 1$
$g > 0$	$\pm$	$+$	$+$
$g < 0$	$\varnothing$	$\varnothing$	$+$

Appendix. Bulk modulational instability

Here a review [54,67,61] of the bulk or potential-free modulational instability results are given for both the scalar and vector versions of Eqs. (6) and (7). In this case, eigenvalue system (31)–(34) can be solved exactly on the domain $[0, d]$ with periodic boundary conditions. For the scalar case ($\beta = 0$) the stability/instability eigenvalues are given by

$$\lambda_n = \pm\omega n\sqrt{\omega^2 n^2 - 2gA^2}, \quad n \in \mathbb{Z} \tag{A.1}$$

where $\omega = 2\pi/d$. The eigenfunctions are unstable when $\lambda_n \in \mathbb{C}$, or equivalently when the intensity satisfies the instability criteria

$$0 < \frac{\omega^2 n^2}{2g} < A^2. \tag{A.2}$$

We point out that this instability condition is only met with focusing ($g > 0$) nonlinearity. Additionally, we observe the absence of unstable modes at low intensities i.e. $A^2 < A^2_{\text{th}}$ given the intensity threshold $A^2_{\text{th}} = 2\pi^2/(gd^2)$. This intensity threshold is lowered by either extending the domain length d or through a stronger attractive nonlinearity g.

Next let us consider the potential free two-component ($\beta \neq 0$) problem on the same periodic domain of length d. The vector situation contains richer variety of parameter regimes corresponding to modulational instability. Here, the four stability eigenvalues are

$$\lambda_n = \pm\omega n\sqrt{\omega^2 n^2 - \mathcal{U}_g \pm \sqrt{\mathcal{U}_g^2 + 4g^2A^2B^2(\beta^2 - 1)}},$$
$$\mathcal{U}_g = g(A^2 + B^2). \tag{A.3}$$

Notice the eigenvalues take an imaginary (unstable) value when

$$0 < \omega^2 n^2 < \mathcal{U}_g \pm \sqrt{\mathcal{U}_g^2 + 4g^2A^2B^2(\beta^2 - 1)}. \tag{A.4}$$

The instabilities can be factored into three scenarios based on the magnitude of the coupling coefficient: weak coupling ($0 < \beta < 1$), balanced coupling ($\beta = 1$), and strong coupling ($\beta > 1$). Based on these three categories and the type of nonlinearity we can determine whether the instability condition in Eq. (A.4) is satisfied for appropriate intensities. These findings are summarized in Table A.1. One of the intriguing observations is the presence of MI under defocusing nonlinearity in the strong coupling regime. This is in contrast to the scalar findings given in Eq. (A.2) where only focusing nonlinearity can cause instability.

References

[1] M.C. Cross, P.C. Hohenberg, Pattern formation outside of equilibrium, Phys. Rev. Mod. Phys. 65 (1993) 851–1112.
[2] T.B. Benjamin, J.E. Feir, The disintegration of wave trains on deep water, J. Fluid Mech. 27 (1967) 417–430.
[3] T.B. Benjamin, Instability of periodic wavetrains in nonlinear dispersive systems, Proc. R. Soc. Lond. Ser. A Math. Phys. Eng. Sci. 299 (1967) 59–76.
[4] A.L. Hodgkin, A.F. Huxley, A quantitative description of membrane current and its application to conduction and excitation in nerve, J. Physiol. 117 (1952) 500–544.
[5] A.S. Davydov, N.I. Kislukha, Solitary excitons in one-dimensional molecular chains, Phys. Status Solidi (B) 59 (1973) 465–470.
[6] T. Taniuti, H. Washimi, Self-trapping and instability of hydromagnetic waves along the magnetic field in a cold plasma, Phys. Rev. Lett. 21 (1968) 209–212.
[7] K. Tai, A. Hasegawa, A. Tomita, Observation of modulational instability in optical fibers, Phys. Rev. Lett. 56 (1986) 135–138.
[8] L. Salasnich, A. Parola, L. Reatto, Modulational instability and complex dynamics of confined matter-wave solitons, Phys. Rev. Lett. 91 (1986) 080405.
[9] R. Malendevich, L. Jankovic, G.I. Stegeman, J.S. Aitchison, Spatial modulation instability in a Kerr slab waveguide, Opt. Lett. 26 (2001) 1879–1881.
[10] H. Fang, R. Malendevich, R. Schiek, G.I. Stegeman, Spatial modulational instability in one-dimensional lithium niobate slab waveguides, Opt. Lett. 25 (2000) 1786–1788.
[11] D. Kip, M. Soljacic, M. Segev, E. Eugenieva, D.N. Christodoulides, Modulation instability and pattern formation in spatially incoherent light beams, Science 290 (2000) 495–498.
[12] J. Meier, G.I. Stegeman, D.N. Christodoulides, Y. Silberberg, R. Morandotti, H. Yang, G. Salamo, M. Sorel, J.S. Aitchison, Experimental observation of discrete modulational instability, Phys. Rev. Lett. 92 (2004) 163902.
[13] V.E. Zakharov, L.A. Ostrovsky, Modulation instability: the beginning, Physica D 238 (2009) 540–548.
[14] V.E. Zakharov, A.M. Rubenchik, Instability of waveguides and solitons in nonlinear media, Sov. Phys.—JETP 38 (1974) 494–500.
[15] B. Deconinck, D.E. Pelinovsky, J.D. Carter, Transverse instabilities of deep-water solitary waves, Proc. R. Soc. Lond. Ser. A Math. Phys. Eng. Sci. 462 (2006) 2039–2061.
[16] D.E. Pelinovsky, E.A. Rouvinskaya, O.E. Kurkina, B. Deconinck, Short-wave transverse instabilities of line solitons of the two-dimensional hyperbolic nonlinear Schrödinger equation, Theoret. Math. Phys. 179 (2014) 452–461.
[17] M.A. Hoefer, B. Ilan, Dark solitons, dispersive shock waves, and transverse instabilities, Multiscale Model. Simul. 10 (2012) 306–341.
[18] G. Theocharis, D.J. Frantzeskakis, P.G. Kevrekidis, B.A. Malomed, Y.S. Kivshar, Ring dark solitons and vortex necklaces in Bose–Einstein condensates, Phys. Rev. Lett. 90 (2003) 120403.
[19] V.A. Brazhnyi, V.M. Pérez-García, Stable multidimensional soliton stripes in two-component Bose–Einstein condensates, Chaos Solitons Fractals 44 (2011) 381–389.
[20] M. Ma, R. Carretero-González, P.G. Kevrekidis, D.J. Frantzeskakis, B.A. Malomed, Controlling the transverse instability of dark solitons and nucleation of vortices by a potential barrier, Phys. Rev. A 82 (2010) 023621.
[21] Z.H. Musslimani, J. Yang, Transverse instability of strongly coupled dark-bright Manakov vector solitons, Opt. Lett. 26 (2001) 1981–1983.
[22] C. Anastassiou, M. Soljačić, M. Segev, E.D. Eugenieva, D.N. Christodoulides, D. Kip, Z.H. Musslimani, J.P. Torres, Eliminating the transverse instabilities of Kerr solitons, Phys. Rev. Lett. 85 (2000) 4888–4891.
[23] Z.H. Musslimani, M. Segev, A. Nepomnyashchy, Y.S. Kivshar, Suppression of transverse instabilities for vector solitons, Phys. Rev. E 60 (1999) R1170–R1173.
[24] Y.S. Kivshar, D.E. Pelinovsky, Self-focusing and transverse instabilities of solitary waves, Phys. Rep. 331 (2000) 117–195.
[25] V.E. Zakharov, A.A. Gelash, Nonlinear stage of modulation instability, Phys. Rev. Lett. 111 (2013) 054101.
[26] A.A. Gelash, V.E. Zakharov, Superregular solitonic solutions: a novel scenario for the nonlinear stage of modulation instability, Nonlinearity 27 (2014) R1–R39.
[27] G. Biondini, D. Mantzavinos, Universal nature of the nonlinear stage of modulational instability, Phys. Rev. Lett. 116 (2016) 043902.
[28] M.J. Ablowitz, D.J. Kaup, A.C. Newell, H. Segur, Method for solving the sine-Gordon equation, Phys. Rev. Lett. 30 (1973) 1262–1264.
[29] G. Theocharis, Z. Rapti, P.G. Kevrekidis, D.J. Frantzeskakis, V.V. Konotop, Modulational instability of Gross–Pitaevskii-type equations in 1+1 dimensions, Phys. Rev. A 67 (2003) 063610.
[30] V.V. Konotop, M. Salerno, Modulational instability in Bose–Einstein condensates in optical lattices, Phys. Rev. A 65 (2002) 021602R.
[31] J.C. Bronski, L.D. Carr, R. Carretero-González, B. Deconinck, J.N. Kutz, K. Promislow, Modulational instability for nonlinear Schrödinger equations with a periodic potential, Phys. Rev. E 64 (2001) 056615.
[32] Z. Rapti, P.G. Kevrekidis, A. Smerzi, A.R. Bishop, Parametric and modulational instabilities of the discrete nonlinear Schrödinger equation, J. Phys. B: At. Mol. Opt. Phys. 37 (2004) S257–S264.
[33] D.N. Christodoulides, R.I. Joseph, Discrete self-focusing in nonlinear arrays of coupled waveguides, Opt. Lett. 13 (1988) 794–796.
[34] M.J. Ablowitz, Z.H. Musslimani, Discrete spatial solitons in a diffraction-managed nonlinear waveguide array: a unified approach, Physica D 184 (2003) 276–303.
[35] K.G. Makris, R. El-Ganainy, D.N. Christodoulides, Z.H. Musslimani, Beam dynamics in PT symmetric optical lattices, Phys. Rev. Lett. 100 (2008) 103904.
[36] R. El-Ganainy, K.G. Makris, D.N. Christodoulides, Z.H. Musslimani, Theory of coupled optical PT symmetric structures, Opt. Lett. 32 (2007) 2632–2634.
[37] Z.H. Musslimani, K.G. Makris, R. El-Ganainy, D.N. Christodoulides, Optical solitons in PT periodic potentials, Phys. Rev. Lett. 100 (2008) 030402.
[38] Z.H. Musslimani, K.G. Makris, R. El-Ganainy, D.N. Christodoulides, Analytical solutions to a class of nonlinear Schrödinger equations with-like potentials, J. Phys. A 41 (2008) 244019.
[39] K.G. Makris, L. Ge, H.E. Türeci, Anomalous transient amplification of waves in non-normal photonic media, Phys. Rev. X 4 (2014) 041044.
[40] C.E. Rüter, K.G. Makris, R. El-Ganainy, D.N. Christodoulides, M. Segev, D. Kip, Observation of parity-time symmetry in optics, Nat. Phys. 6 (2010) 192–195.
[41] A. Guo, G.J. Salamo, D. Duchesne, R. Morandotti, M. Volatier-Ravat, V. Aimez, G.A. Siviloglou, D.N. Christodoulides, Observation of PT-symmetry breaking in complex optical potentials, Phys. Rev. Lett. 103 (2009) 093902.

[42] A. Regensburger, C. Bersch, M.-A. Miri, G. Onishchukov, D.N. Christodoulides, U. Peschel, Parity-time synthetic photonic lattices, Nature 488 (2012) 167–171.
[43] C.M. Bender, S. Boettcher, Real Spectra in non-hermitian Hamiltonians having PT symmetry, Phys. Rev. Lett. 80 (1998) 5243–5246.
[44] C.M. Bender, Making sense of non-hermitian Hamiltonians, Rep. Progr. Phys. 70 (2007) 947–1018.
[45] A. Regensburger, M.A. Miri, C. Bersch, J. Näger, G. Onishchukov, D.N. Christodoulides, U. Peschel, Observation of defect states in PT-symmetric optical lattices, Phys. Rev. Lett. 110 (2013) 223902.
[46] Z. Lin, H. Ramezani, T. Eichelkraut, T. Kottos, H. Cao, D.N. Christodoulides, Unidirectional invisibility induced by PT-symmetric periodic structures, Phys. Rev. Lett. 106 (2011) 213901.
[47] M. Liertzer, L. Ge, A. Cerjan, A.D. Stone, H.E. Türeci, S. Rotter, Pump-induced exceptional points in lasers, Phys. Rev. Lett. 108 (2012) 173901.
[48] M. Brandstetter, M. Liertzer, C. Deutsch, P. Klang, J. Schöberl, H.E. Türeci, G. Strasser, K. Unterrainer, S. Rotter, Reversing the pump dependence of a laser at an exceptional point, Nat. Commun. 5 (2014) 4034.
[49] N. Bender, S. Factor, J.D. Bodyfelt, H. Ramezani, D.N. Christodoulides, F.M. Ellis, T. Kottos, Observation of asymmetric transport in structures with active nonlinearities, Phys. Rev. Lett. 110 (2013) 234101.
[50] F. Nazari, N. Bender, H. Ramezani, M.K. Moravvej-Farshi, D.N. Christodoulides, T. Kottos, Optical isolation via PT-symmetric nonlinear Fano resonances, Opt. Express 22 (2014) 9574–9584.
[51] K.G. Makris, Z.H. Musslimani, D.N. Christodoulides, S. Rotter, Constant-intensity waves and their modulation instability in non-Hermitian potentials, Nat. Commun. 6 (2015) 7257.
[52] H. Segur, D. Henderson, J. Carter, J. Hammack, C.-M. Li, D. Pheiff, K. Socha, Stabilizing the Benjamin-Feir instability, J. Fluid Mech. 539 (2005) 229–271.
[53] F. Kh. Abdullaev, J. Garnier, Modulational instability of electromagnetic waves in birefringent fibers with periodic and random dispersion, Phys. Rev. E 60 (1999) 1042–1050.
[54] G.P. Agrawal, Nonlinear Fiber Optics, Academic Press, 2012.
[55] Z.G. Chen, M. Segev, T.H. Coskun, D.N. Christodoulides, Y.S. Kivshar, Incoherently coupled dark-bright photorefractive solitons, Opt. Lett. 21 (1996) 1821–1823.
[56] Z.G. Chen, M. Segev, T.H. Coskun, D.N. Christodoulides, Observation of incoherently coupled photorefractive spatial soliton pairs, Opt. Lett. 21 (1996) 1436–1438.
[57] B. Deconinck, J.N. Kutz, Computing spectra of linear operators using the Floquet-Fourier-Hill method, J. Comput. Phys. 219 (2006) 296–321.
[58] J. Yang, Nonlinear Waves in Integrable and Nonintegrable Systems, SIAM, Philadelphia, 2010.
[59] L.N. Trefethen, Spectral Methods in MATLAB, SIAM, Philadelphia, 2000.
[60] M.S.P. Eastham, The Spectral Theory of Periodic Differential Equations, Scottish Academic Press, 1973.
[61] J.A.C. Weideman, B.M. Herbst, Split-step methods for the solution of the nonlinear Schrödinger equation, SIAM J. Numer. Anal. 23 (1986) 485–507.
[62] J. Meier, J. Hudock, D.N. Christodoulides, G. Stegeman, Y. Silberberg, R. Morandotti, J.S. Aitchison, Discrete vector solitons in Kerr nonlinear waveguide arrays, Phys. Rev. Lett. 91 (2003) 143907.
[63] X. Liu, H. Pu, B. Xiong, W.M. Liu, J. Gong, Formation and transformation of vector solitons in two-species Bose–Einstein condensates with a tunable interaction, Phys. Rev. A 79 (2009) 013423.
[64] D. Feijoo, Á. Paredes, H. Michinel, Outcoupling vector solitons from a Bose–Einstein condensate with time-dependent interatomic forces, Phys. Rev. A 87 (2013) 063619.
[65] G. Csire, D. Schumayer, B. Apagyi, Effect of scattering lengths on the dynamics of a two-component Bose–Einstein condensate, Phys. Rev. A 82 (2010) 063608.
[66] I.V. Barashenkov, D.A. Zezyulin, V.V. Konotop, Exactly solvable Wadati potentials in the PT-symmetric Gross–Pitaevskii equation, 2015. arXiv:1511.06633.
[67] G.P. Agrawal, P.L. Baldeck, R.R. Alfano, Modulational instability induced by cross-phase modulation in optical fibers, Phys. Rev. A 82 (1989) 3406–3413.